This article has been accepted for publication in a future issue of this journal, but has not been fully edited. Content may change prior to final publication. Citation information: DOI 10.1109/TIA.2018.2819968, IEEE Transactions on Industry Applications

A New Design Method of an LCL Filter Applied in Active DC-Traction Substations

Mihaela Popescu, *Senior Member*, *IEEE*, Alexandru Bitoleanu, *Senior Member, IEEE*, and Alexandra Preda

***Abstract*—This paper concentrates on the LCL filter with damping resistance intended to connect the shunt active power filter of an active DC-traction substation to the point of common coupling with the transmission grid. In order to find design conditions and conceive a design algorithm, attention is directed to the transfer functions related to currents and the associated frequency response. The mathematical foundation of the design method is based on the meeting the requirements related to the significant attenuation of the high-frequency switching current, concurrently with the unalterated flow of the current that needs to be compensated by active filtering. It is pointed out that there are practical limitations and a compromise must be made between the two requirements. To quantify the extent to which the harmonics to be compensated are influenced by imposing the magnitude response at both highest harmonic frequency to be compensated and switching frequency, a performance indicator is defined. As an additional design criterion, the damping power losses are taken into consideration. The validity and effectiveness of the proposed method are proved by simulation results and experimental tests on a laboratory test bench of small scale reproducing the specific conditions of a DC-traction substation with six-pulse diode rectifier.**

***Index Terms*—DC-traction substations, LCL filter, passive damping, regeneration, shunt active power filters.**

I. INTRODUCTION

The issue of connecting the power inverters to the AC power supply through a passive interface filter, allowing the injected current to be free of high order switching harmonics, has attracted the attention of the specialists in recent years. Compared to the simple L filter, the higher order LCL filter is a more attractive solution due to the improved performance, accompanied by lower value of needed inductances, the overall size and cost.

Most investigations on the LCL filter design are related to its connection at the output of simple power supply-tied voltage source inverters (VSIs), where the global control strategy is mainly directed to the fundamental frequency. Achieving stable operation, avoiding the unwanted resonance and slow dynamic response are challenging tasks [1]–[13]. Several characteristics are considered in designing the LCL filter, such as current ripple, power factor variation seen by the grid, and switching ripple attenuation [7]. A generalized design algorithm for grid-connected LCL filter, to satisfy the required switching frequency attenuation and the reactive power compensation limits, is proposed in [8], where the exact position of the resonance frequency is identified. In [12], a comprehensive minimum-weight LCL filter design procedure is proposed, incorporating the parameters selection, current control, damping limits, stability margin, semiconductor power losses, and cooling conditions.

Developing models for grid-connected VSIs, including the LCL filter, is another concern, facilitating the design and validation of advanced control strategies. Different models with different combinations of simplifications are discussed in [13], which is mainly directed to the state-space-based modeling.

Many kinds of passive-damped filters used as interface between VSI and the utility grid, are recently reviewed and then evaluated in [9], in terms of damping capability and power loss in the damping circuit. In order to reduce the system volume and cost, a magnetic integrated LLCL filter for grid-connected VSI is proposed in [10]. As expressed, compared to the conventional LCL filter, a reduction of the filter inductance by 50 % can be expected.

For the practical case of using the passive-damped LCL filter to interface a voltage source converter acting as active rectifier operating in rectifying and regenerating-mode, the design procedure proposed in [11] uses the power rating of the converter, the switching frequency, and the required current ripple on the converter side as inputs.

When connected to the output of VSI acting as shunt active power filter (SAPF), the LCL filter design faces new challenges, as the harmonics to be compensated should pass without alteration, while the switching harmonics should be attenuated significantly. Few papers in literature are addressed to this concrete application, compared to the general case of VSI. To handle the possible instability, the existing damping methods involve either the adding a resistor in series with the filter capacitor or adopting an active damping technique through a specific control of the system.

A comprehensive approach to designing the SAPF's interconnecting LCL-filter with passive damping resistor is given in [14], where certain decisions are taken about the total inductance, region for the resonance frequency and the capacitance.

Based on the LCL filter structure, a high order passive damping LLCL filter with a small inductor inserted in the capacitor branch to obtain very low impedance at the switching frequency is the solution adopted in [15] for coupling the SAPF to the power supply.

In [16], the active damping technique through the control strategy is considered and a generalized design procedure for an LCL-filter-based SAPF is proposed in per-unit terms, where the grid and converter-side inductances are set to be equal. Moreover, the total per unit value of the two inductances are chosen equal to that of the filter capacitor. Focused on a three-level SAPF, the authors of [17] initiate the design process of the LCL filter with damping resistor by

This article has been accepted for publication in a future issue of this journal, but has not been fully edited. Content may change prior to final publication. Citation information: DOI 10.1109/TIA.2018.2819968, IEEE Transactions on Industry Applications

choosing the resonance frequency in accordance with the highest order harmonic needed to be compensated and then follow the recommendations of [16]. In [18], suitable parameters of a single-phase grid-connected LCL filter are obtained through the graph determined by expected performance indexes. The limitations of both the inverter-side and power supply-side current magnitude attenuation coefficients are introduced in order to decouple the relations between the filter parameters and the performance indexes.

There are very few references to the passive coupling filters in the traction systems with improved power quality by implementing the parallel compensation techniques or with parallel regeneration units. The hybrid solution proposed in [19] to mitigate the power quality problems in Light Rail public Transportation Systems includes a second-order low-pass filter whose design is discussed. Reference [20] presents the practical implementation of a unit for active regeneration in the Rotterdam metro network, where the drawbacks of the adopted LC line filter are pointed out and the possibility of replacing it with a more efficient LCL filter is expressed.

In our opinion, a unified approach to the design of the interface filter by taking into consideration the influence of its parameters, including damping resistance, must start from the fact that the SAPF acts as a current source providing harmonic currents to a low-pass wideband passive filter. Therefore, the attention should be directed mainly to the transfer functions related to currents. In contradistinction to this approach, many papers are focused on transfer functions as admittances or impedance characteristics [15], [16], [18], [21]–[24].

In this paper, a new design method of the LCL filter with damping resistance to connect a SAPF to PCC is proposed. The practical application taken into consideration is an active DC-traction substation with uncontrolled rectifier [25]–[28]. After introducing the structure of the active DC-traction substation (Section II) followed by the voltage and current control (Section III), Section IV is directed to the transfer functions and the frequency response of the LCL filter. Next, the study of the behavior and performance of the interface filter, leading to some design aspects and limitations, is resulted based on the functions to be performed during operation. The proposed design algorithm in Section VI is followed by the presentation of the filtering performance obtained by simulation and experimentation in the practical case of an active DC-traction substation with six-pulse diode rectifier. Some concluding remarks are drawn at the end of the paper.

II. Structure of the Active DC-Traction Substation

As shown in Fig. 1, the existing DC-traction substation with uncontrolled rectifier becomes an active substation by adding a VSI-based SAPF in anti-parallel with the traction rectifier, via a separating circuit on the DC-side and a coupling circuit on the AC-side. In this manner, the braking energy recovery is allowed and the improvement of power quality by active filtering is possible during the traction regime [20].

The separating circuit consisting of a diode in series with an inductor split into two identical parts ensures the decoupling of SAPF from the DC-line during the operation in traction regime in order to achieve the function of active filtering and acts as an energy buffer during the operation in regeneration regime.

To ensure the current dynamics and sufficiently smooth the SAPF's output currents affected by the switching frequency harmonics, an LCL filter with damping resistors interfaces the connection to the point of common coupling (PCC) with the power supply.

In choosing the proper PCC, it must be taken into account that the rated DC-line voltage must exceed the magnitude of the line-to-line voltage at the SAPF output, in order to inject a good quality current into the AC-line. Thus, when the traction transformer (TT) secondary is taken into consideration as a possible PCC, the above-expressed condition is accomplished only in the case of the 12 pulse series rectifier.

When the traction substation is equipped with a six pulse rectifier or 12 pulse parallel rectifier, a well-designed recovery transformer (RT) ensures the coupling condition, so that PCC becomes the primary of TT (PCC_1 in Fig. 1) [25].

The control scheme proposed to provide the gating signals for IGBTs (Fig. 2) involves the indirect control of the SAPF's output currents by means of the supply currents upstream of PCC [21].

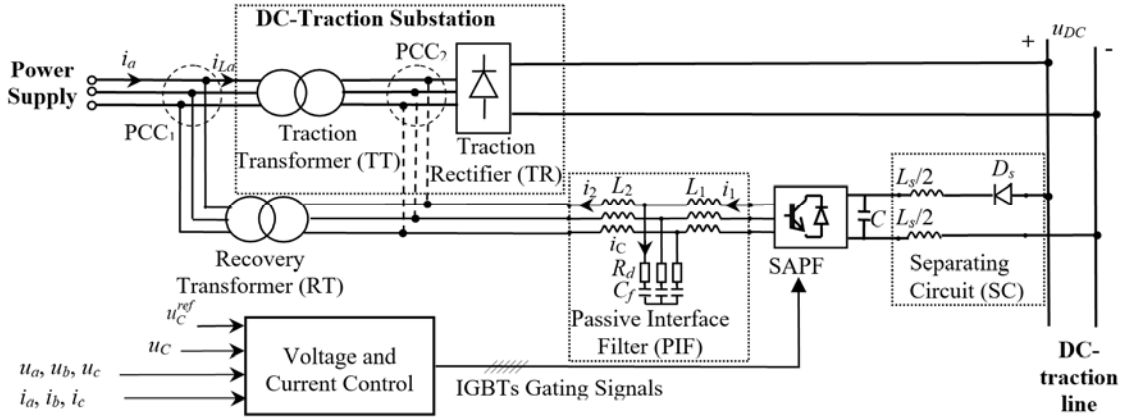

Fig. 1. Block diagram of the active DC-traction substation.

This article has been accepted for publication in a future issue of this journal, but has not been fully edited. Content may change prior to final publication. Citation information: DOI 10.1109/TIA.2018.2819968, IEEE Transactions on Industry Applications

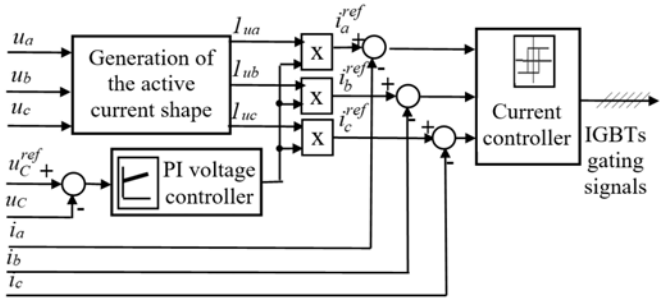

Fig. 2. Block diagram of the control system.

Thus, depending on the scheme of the traction rectifier, the supply currents (i_a, i_b, i_c) and voltages (u_a, u_b, u_c) in Fig. 1 are associated either to the primary or secondary of TT. The same applies for the load currents (i_{La}, i_{Lb}, i_{Lc}). The reference supply currents during the active filtering regime are generated based on the measured AC voltages and DC-capacitor voltage. Synthetically, a voltage controller of proportional-integral (PI) type provides the magnitude of the set currents, whereas a phase locked loop (PLL) circuit supplies their sinusoidal shape [26].

In traction regime, when the DC-line is fed by TR and Ds is blocked, by handling the DC-capacitor voltage, the generated reference supply currents will be active currents, in phase with the supply voltages. In braking regime, when TR is blocked and Ds is forward-biased, the voltage controller is saturated and provides the maximum magnitude of the regenerating current. The reference currents will be active currents, in phase opposition with the supply voltages. Thus, the transition between the two regimes occurs naturally, by the control of the DC-capacitor voltage.

A hysteresis band controller ensures their accurate tracking by the actual supply currents. In the practical discrete-time implementation, by proper fixed sampled time and hysteresis bandwidth, the maximal switching frequency is controlled to be below the IGBTs' capability (about 10 kHz).

III. Voltage and Current Control

The structure of the control system (Fig. 2) illustrates the inner and outer control loops, where the inner one is associated to the supply current and uses a hysteresis band controller providing the needed IGBTs gating signals.

The outer control loop based on a PI voltage controller is aimed to keep the DC-capacitor voltage at its prescribed value. As it was proved in [26], the active current exchanged by the capacitor with the AC power supply is directly proportional to the DC-voltage ripple, so that the DC-voltage ripple can be used to estimate the active supply current. Thus, the magnitude of the sinusoidal prescribed currents at the current controller input is given by the voltage controller. During the traction regime of the vehicle (active filtering for the system), the output signal of the voltage controller has the sign "+", whereas during the braking regime of the vehicle (regeneration for the system), the output signal of the voltage controller has the sign "-".

As regards the sinusoidal shapes of unity magnitude of the prescribed active currents (signals l_{ua}, l_{ub}, l_{uc}), they are synchronized with the supply phase voltages in order to obtain unity power factor, and are provided by a specific PLL circuit whose operation is based on the cancellation of an internal fictitious power [26].

As the optimization is a powerful tool to design controllers and the transfer function in the forward path of the voltage control loop has a simple pole in origin, the PI voltage controller has been designed according to the Symmetrical Optimum criterion [29].

IV. LCL Filter Transfer Functions and Frequency Response

Considering the structure of the LCL filter with damping resistors (Fig. 1) and the equivalent scheme for high order harmonics (Fig. 3) [28], [30], the following transfer functions between the input current i_1 and output currents i_2 and i_C can be expressed as follows:

$$G_1(s)=\frac{I_2(s)}{I_1(s)}=\frac{1+sR_dC_f}{1+sR_dC_f+s^2L_2C_f}; \quad (1)$$

$$G_2(s)=\frac{I_C(s)}{I_1(s)}=\frac{s^2L_2C_f}{1+sR_dC_f+s^2L_2C_f}. \quad (2)$$

It must be specified that, by neglecting the low values of the internal resistances of the inductors and capacitor, the worst scenario in terms of damping is obtained.

All information related to filter performance is provided by the two transfer functions $G_1(s)$ and $G_2(s)$. Indeed, the correct operation of the active filtering system involves the following:

- The current i_1 at the SAPF output contains the current harmonics to be compensated together possibly with the component associated to the reactive power compensation, but also the high order harmonics associated to the switching frequency f_{sw};
- The current i_C through capacitor should contain as much of switching harmonics and as little of harmonics to be compensated;
- Only the harmonics to be compensated should be included in the current i_2 at the filter output.

As a first finding, both transfer functions are not dependent on the inverter-side inductance L_1.

Based on (1), the amplitude response and the resonance frequency (ω_{res}) associated to $G_1(s)$ can be expressed by highlighting their dependence on only pairs L_2C_f and R_dC_f [27], [28], [31]:

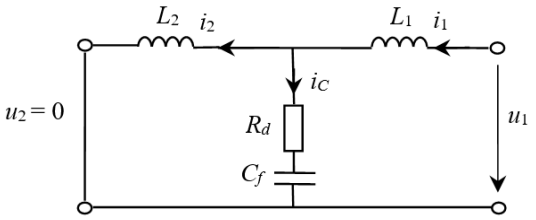

Fig. 3. Equivalent scheme of the LCL filter with damping resistor, for high order harmonics.

This article has been accepted for publication in a future issue of this journal, but has not been fully edited. Content may change prior to final publication. Citation information: DOI 10.1109/TIA.2018.2819968, IEEE Transactions on Industry Applications

$$|G_1(j\omega)| = \sqrt{\frac{1+(R_dC_f)^2\omega^2}{(1-L_2C_f\omega^2)^2+(R_dC_f)^2\omega^2}}\ ; \quad (3)$$

$$\omega_{res} = \frac{1}{R_dC_f}\sqrt{\sqrt{1+\frac{2(R_dC_f)^2}{L_2C_f}}-1}\ . \quad (4)$$

This aspect is useful in the filter design [28].

V. Passive Filter Behavior and Performance

In order to identify the design conditions, the behavior of the passive interface filter must be correlated with the following two functions to be performed:

- To allow the harmonics up to the highest compensated frequency (f_N=50·N) to pass towards the power supply, where the highest order N is imposed mainly by the load current harmonic spectrum, but also by the existing standards;
- To attenuate as much as possible the switching harmonics.

As it will be further pointed out, it is not possible to obtain simultaneously zero attenuation for $f \le f_N$ and very high attenuation at f_{sw}. Thus, if the magnitude (in decibels - dB) for f_{sw} is imposed to be A_{sw} (A_{sw}<0), it means:

$$|G_1(j\omega_{sw})| = 10^{A_{sw}/20}\ , \quad (5)$$

or, based on (3),

$$|G_1(j\omega_{sw})|^2 = \frac{1+(R_dC_f)^2\omega_{sw}^2}{(1-L_2C_f\omega_{sw}^2)^2+(R_dC_f)^2\omega_{sw}^2} = 10^{\frac{A_{sw}}{10}} = \alpha_{sw}\ , (6)$$

where $0<\alpha_{sw}<1$.

Similarly, by imposing the magnitude (dB) for f_N to be A_N ($A_N \ge 0$), it leads to:

$$|G_1(j\omega_N)|^2 = \frac{1+(R_dC_f)^2\omega_N^2}{(1-L_2C_f\omega_N^2)^2+(R_dC_f)^2\omega_N^2} = 10^{\frac{A_N}{10}} = \alpha_N\ , \quad (7)$$

where $\alpha_N \ge 1$.

Expressions (6) and (7) give a system of two equations and variables L_2C_f and R_dC_f providing the following equation:

$$\omega_N^2\omega_{sw}^2\left[\alpha_{sw}(\alpha_N-1)\omega_{sw}^2+\alpha_N(1-\alpha_{sw})\omega_N^2\right](L_2C_f)^2 - \\ -2(\alpha_N-\alpha_{sw})\omega_N^2\omega_{sw}^2L_2C_f+(1-\alpha_{sw})(\alpha_N-1)(\omega_{sw}^2-\omega_N^2)=0 \quad (8)$$

along with the following limitations resulted from the condition to obtain a positive value for R_d:

$$L_2C_f > LC_{i1}\ ;\quad LC_{i1} = \frac{1+\sqrt{\alpha_{sw}}}{\omega_{sw}^2\sqrt{\alpha_{sw}}}\ ; \quad (9)$$

$$L_2C_f \in [LC_{i2}, LC_s]\ ;\ LC_{i2} = \frac{\sqrt{\alpha_N}-1}{\omega_N^2\sqrt{\alpha_N}}\ ;\ LC_s = \frac{\sqrt{\alpha_N}+1}{\omega_N^2\sqrt{\alpha_N}}\ . (10)$$

The discriminant Δ of the quadratic equation (8) is:

$$\Delta = 4\cdot\left\{\omega_N^4\omega_{sw}^4(\alpha_N-\alpha_{sw})^2-\omega_N^2\omega_{sw}^2(1-\alpha_{sw})\cdot(\alpha_N-1)\cdot \right. \\ \left.\cdot(\omega_{sw}^2-\omega_N^2)\cdot\left[\alpha_{sw}\omega_{sw}^2(\alpha_N-1)+\alpha_N\omega_N^2(1-\alpha_{sw})\right]\right\} \quad (11)$$

and must be positive or null in order to obtain real solutions for L_2C_f. Starting from this condition, the graph in Fig. 4 shows that, for each imposed amplification A_N corresponding to an imposed value of $|G_1(j\omega_N)|$ in the domain [1÷1.2], there is a domain of A_{sw} for which $\Delta \ge 0$.

The practical case study of N = 51 and f_{sw} =10 kHz will be further taken into consideration.

It can be seen that, for the large area $A_N \in$ [0, 1.3] and $A_{sw} \in$[-25, -5], the discriminant is positive (Fig. 4).

As illustrated in Fig. 5, only the solution

$$(L_2C_f)_1 = \frac{2(\alpha_N-\alpha_{sw})\omega_N^2\omega_{sw}^2+\sqrt{\Delta}}{2\omega_N^2\omega_{sw}^2\left[\alpha_{sw}(\alpha_N-1)\omega_{sw}^2+\alpha_N(1-\alpha_{sw})\omega_N^2\right]} \quad (12)$$

fulfills conditions (9) and (10).

On the other hand, the resonance frequency (4) and the associated magnitude response depend only on the pairs L_2C_f and R_dC_f, whose values are determined by the imposed values for A_N and A_{sw} (Fig. 6). Thus, the resonance frequency is very close or below the frequency of maximal order taken into consideration to be compensated, involving an unwanted amplification of some harmonics of order below N (Fig. 7). Moreover, the amplification for ω_{res} is high when the imposed attenuation for ω_{sw} is high (Fig. 6 (b)).

In order to obtain additional design criteria, the power losses P_d on the damping resistance were taken into consideration. Assuming the ideal operation of the passive filter, only the switching currents pass through the damping resistances in series with capacitors.

Taking into consideration the fundamental rms switching current I_C and (2), the power losses are expressed as [27]:

$$P_d = 3R_dI_C^2 = 3R_d\frac{(\omega_{sw}^2L_2C_f)^2}{(1-\omega_{sw}^2L_2C_f)^2+\omega_{sw}^2R_d^2C_f^2}I_1^2\ . \quad (13)$$

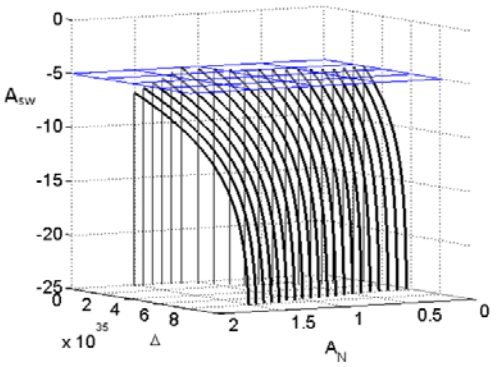

Fig. 4. Dependence between A_{sw}, A_N and positive Δ.

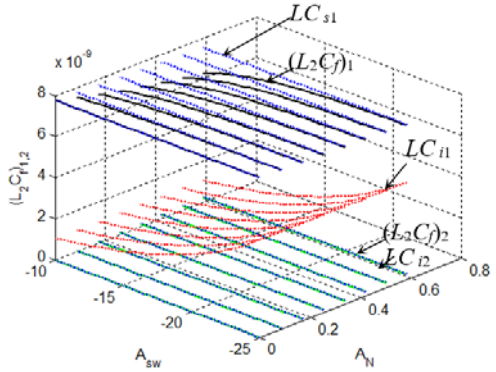

Fig. 5. Solutions $(L_2C_f)_{1,2}$ of (8) and their limits as a function of A_N and A_{sw}.

This article has been accepted for publication in a future issue of this journal, but has not been fully edited. Content may change prior to final publication. Citation information: DOI 10.1109/TIA.2018.2819968, IEEE Transactions on Industry Applications

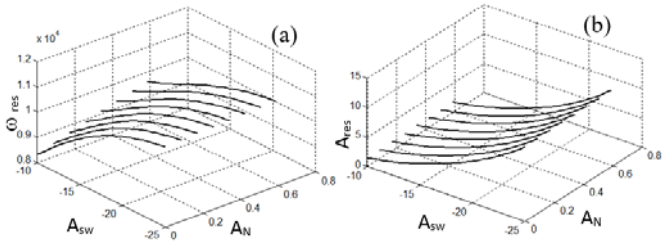

Fig. 6. Resonance frequency (rad/s) (a) and the associated amplification (b) as a function of A_N and A_{sw}.

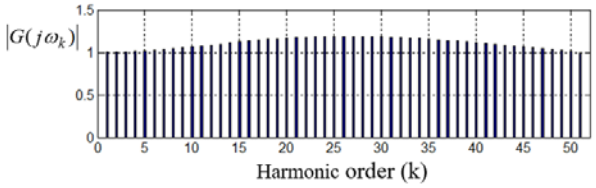

Fig. 7. Magnification of the harmonics up to N=51, for A_N=0, A_{sw}=-10, and C_f=15µF.

It shows that, for a given rms current at the filter input and imposed values for A_N and A_{sw} (i.e. known L_2C_f and R_dC_f), low values of the losses are obtained for a low value of R_d and high value of C_f. Thus, the ratio

$$P_d / I_1^2 = 3R_d \frac{(\omega_{sw}^2 L_2 C_f)^2}{(1-\omega_{sw}^2 L_2 C_f)^2 + \omega_{sw}^2 R_d^2 C_f^2} = R_{ech}, \quad (14)$$

which can be seen as an equivalent resistance, is an indicator of power losses.

To quantify the extent to which the harmonics to be compensated are influenced by imposing the magnitude response at f_N and f_{sw}, the following magnitude performance indicator is proposed:

$$MPI = \sqrt{\sum_{k=1}^{N} \left(|G(j\omega_k)|/k\right)^2 \Big/ \sum_{k=1}^{N} \left(1/k^2\right)}. \quad (15)$$

Therefore, the more the value of *MPI* is closer to 1, the better filter performance is obtained. It must be specified that, by using the square of the harmonic magnitudes in the numerator of (15), the weight of the amplified harmonics is favored, compared to that of the attenuated harmonics. Moreover, each harmonic magnitude is divided by the harmonic order, to favor the weight of low order harmonics.

The Bode plots in Fig. 8 show that the passive filter behavior concerning the harmonics to be compensated can be improved if the accepted attenuation $|A_{sw}|$ at f_{sw} is not so great as wanting and the power losses can be decreased by accepting a small amplification at frequency f_N.

VI. Design Method

Based on the above analysis and mathematical foundation, the proposed design method for the passive interface filter involves determining the best variant of parameters in terms of indicator *MPI,* of the best variants in terms of indicator R_{ech}. Specifically, the following steps must be completed.

1. Analyze the distorted load current and determine the highest order N of the harmonics that needs to be compensated by SAPF and the associated frequency f_N.

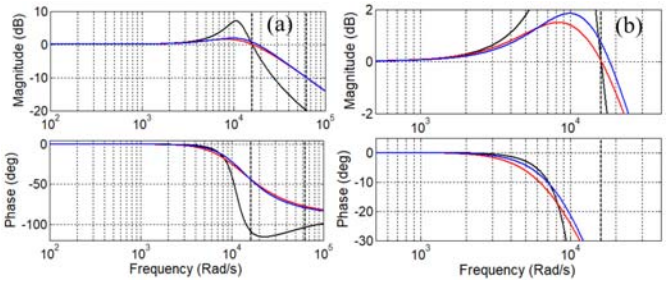

Fig. 8. Bode diagrams (a) and details on them (b) for N=51, different imposed pairs (A_N, A_{sw}) and values of filter parameters: A_N=0, A_{sw}=-20, C_f=15µF, L_2=0.52mH, R_d=2.98Ω, R_{ech}=9.49Ω, *MPI*=1.03 (black line); A_N=0.7, A_{sw}=-10, C_f=5µF, L_2=1.2mH, R_d=23.98Ω, R_{ech}=70.7Ω, *MPI* = 1.0107 (blue line); A_N=0, A_{sw}=-10, C_f=5µF, L_2=1.56mH, R_d=31.39Ω, R_{ech}=90.6Ω, *MPI*=1.0108 (red line).

2. Determine the switching frequency f_{sw} depending on the power switching devices and the existing control method.

3. From an established area of acceptable values, impose the attenuation A_{sw} (dB) for the switching frequency and calculate α_{sw}.

4. From an established area of acceptable values, impose the attenuation A_N (dB) for f_N and calculate α_N.

5. Calculate the product L_2C_f as the solution (12) of equation (8).

6. Impose a value for C_f.

7. Calculate the needed value of R_d based on condition (6), i.e.:

$$R_d = \frac{1}{\omega_{sw} C_f} \sqrt{\frac{\alpha_{sw}(1-\omega_{sw}^2 L_2 C_f)^2 - 1}{1-\alpha_{sw}}}. \quad (16)$$

8. Calculate the value of L_2 based on the product L_2C_f obtained at step 5.

9. Based on the Bode magnitude diagram and (15), calculate the indicator *MPI*.

10. Calculate the equivalent resistance R_{ech} by (14), as an indicator of power losses.

11. Go through the steps 7-10 for several values of C_f.

12. Retain the sets of values (C_f, R_d, L_2) and the associated *MPI*, for which R_{ech} is minimal.

13. Go through the steps 3-12 for other values of A_{sw} and A_N respectively.

14. From the values retained at step 12, adopt the set (C_f, R_d, L_2) for which the indicator *MPI* is the closest to 1.

As regards the inverter-side inductance L_1, it does not intervene in the transfer functions related to currents and can be designed so that the switching losses in the inverter's semiconductor devices to be limited.

Other criteria in the literature refer to the following: limiting the voltage drop on it [2] or on the total inductance [17], [22]; avoiding the inductor saturation [6]; imposing the current ripple at the VSI output [7], [9], [11], [12], [18], [21]; adopting L_1=L_2 ([8], [16]) and then the design of the total inductance [8] or imposing the per unit inductance to bring down the system cost [16]; limiting the maximum switching frequency [14].

In our approach, in order to limit the switching losses in IGBTs, the minimum required inductance has been taken into

This article has been accepted for publication in a future issue of this journal, but has not been fully edited. Content may change prior to final publication. Citation information: DOI 10.1109/TIA.2018.2819968, IEEE Transactions on Industry Applications

consideration, based on the relationship between the maximum switching frequency, the DC-link voltage, the hysteresis band and the total inductance [14].

VII. Performance of the System for Active Filtering and Regeneration

A. Simulation Results

To verify the proper behavior and evaluate the performance of the passive-damped LCL filter in coupling the SAPF of an active DC-traction with six-pulse parallel diode rectifier to the power supply, the Matlab/Simulink model of the whole system has been conceived. It uses the real structure of the system, in accordance with Fig. 1. The parameters correspond to a small scale setup associated to the conceived laboratory test bench, in order to compare the simulation and experimental results. The main parameters of the power system are included in Table I.

In modeling the traction DC-line, it was taken into consideration that, in traction regime, it is an active load with a back electromotive force associated to the operation speed and equivalent parameters (resistance and inductance) of the traction motors and DC-line. In regeneration-mode, by imposing a constant acceleration and a maximal DC-line voltage, the DC-line current is constant [26].

The waveforms of currents in the TT's primary in traction regime (Fig. 9) and the associated harmonic spectrum (Fig. 10) illustrate the need for harmonic and reactive power compensation. The total harmonic distortion factor (*THD*) is 23.7% and the global power factor is 0.94. Moreover, the harmonics of order over 37 are below 0.5 % of the fundamental component (Fig. 10).

TABLE I
Main Parameters of the System

Items	Values
Rated apparent power (S_N)	30 kVA
AC system voltage (U_N)	380 V
Traction transformer (connection Y/y)	380 V/ 150 V ; R_1=0.292 Ω; R_2=0.045 Ω; R_m=2.57 kΩ; $L_{σ1}$=1.5 mH ; $L_{σ2}$=0.23 mH; L_m=1.03 H
Recovery transformer (connection Y/d)	380 V/130 V; R_1=0.966 Ω; R_2=0.337 Ω; R_m =566.83 Ω; $L_{σ1}$=3.1 mH; $L_{σ2}$=1.1 mH; L_m=4.682 H
Rated DC-line voltage (U_{DCN})	190 V
DC-link capacitance (C)	2200 µF
Inductance of the DC-separating circuit (L_s)	4.9 µH
PI voltage controller parameters	K_p=3.53; T_i=1.8·10^{-3} s
Hysteresis band of the current controller	0.75 A

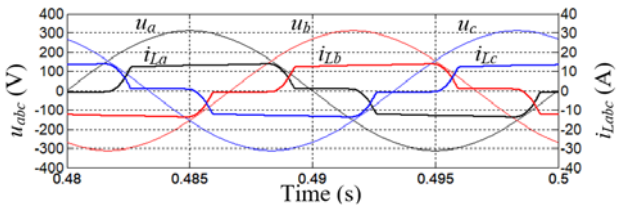

Fig. 9. Voltages and currents in the TT's primary in traction regime.

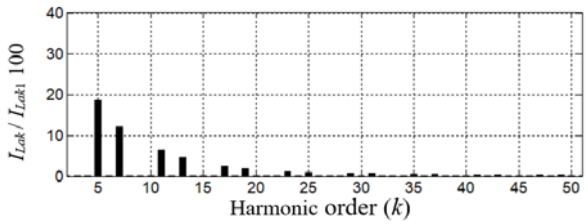

Fig. 10. Harmonic spectrum of the current in the primary of TT.

Thus, the harmonic of order 37 can be considered as the last significant harmonic to be compensated.

Taking into consideration that f_{sw}=10 kHz and N=37, the proposed design algorithm provides the following parameters of the LCL filter: C_f=10 µF; R_d=27 Ω; L_2=1.48 mH. They correspond to the imposed the attenuation A_N =0 dB and A_{sw} = -11 dB.

The resulted value for *MPI* is 1.01 and the associated indicator of the power losses is R_{ech}=76.64 Ω, which represents about 54% of the maximum value of 141.94 Ω.

A small inverter-side inductance, L_1=34 µH, is adopted, to limit the IGBTs' switching losses, using the relationship between the DC-link voltage, hysteresis band, total inductance and maximum switching frequency [14].

The associated Bode magnitude diagram (Fig. 11) shows the inevitable low amplification of some harmonic close to order N.

By prescribing the proper reference current for total compensation (current harmonics and reactive power), the SAPF provides a current at the LCL filter input (Fig. 12) which is affected by the inverter switching.

The current flowing through the capacitor of the interface filter is shown in Fig. 13 and the harmonic spectra of input and output currents (Fig. 14) illustrate the insignificant influence of the interface filter on the harmonics up to N= 37. It must be notified that the existence of the fundamental component corresponds to the necessity of reactive power compensation.

The LCL filter fulfills its mission to reduce significantly the switching component of the current, so that the current upstream of PCC is close to a sinusoide (Fig. 15), having a total harmonic distortion of about 2.37%. Moreover, almost unity power factor (0.999) is obtained, as the fundamental of the supply current has the same phase as the supply voltage.

The waveforms of the supply current and voltage when the active traction substation operates successively in traction (active filtering) and braking (regeneration) regimes (Fig. 16) confirm the proper behavior and good performance of the system, including the appropriate interface filter.

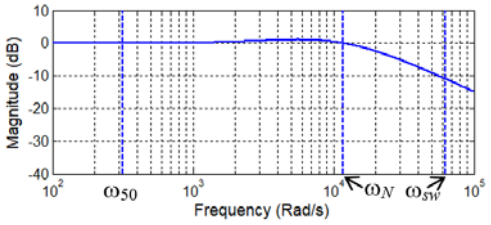

Fig. 11. Bode magnitude diagram for C_f =10µF, R_d =27Ω; L_2 =1.48mH.

This article has been accepted for publication in a future issue of this journal, but has not been fully edited. Content may change prior to final publication. Citation information: DOI 10.1109/TIA.2018.2819968, IEEE Transactions on Industry Applications

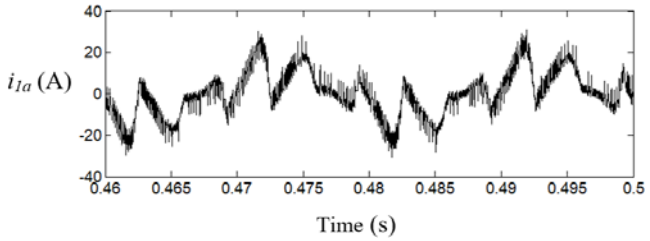

Fig. 12. LCL filter input current.

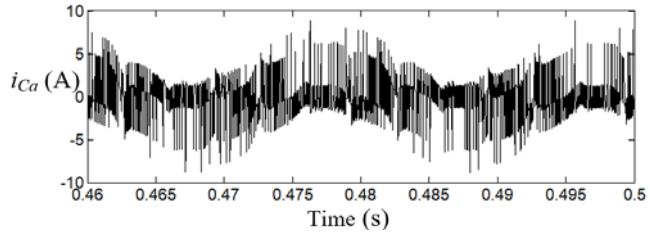

Fig. 13. Current flowing through the capacitor of the interface filter.

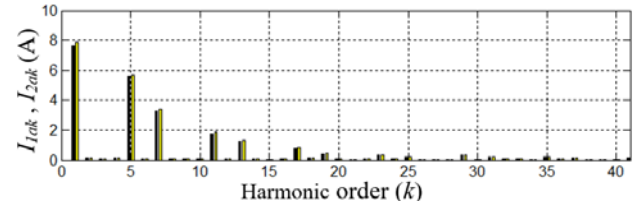

Fig. 14. Harmonic spectra of the LCL filter input current (black bars) and output current (yellow bars) for harmonic order $k \in [1, 37]$.

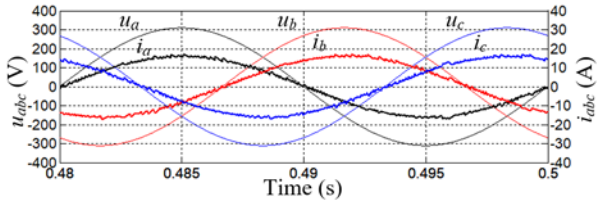

Fig. 15. Voltages and currents upstream of PCC during the operation in traction regime.

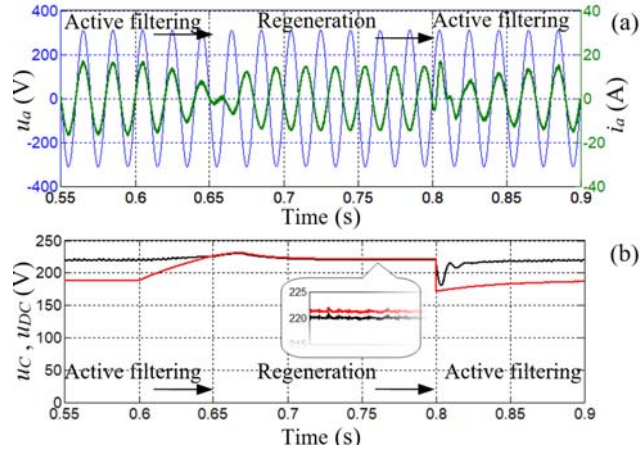

Fig. 16. Succesive traction (filtering) and braking (regeneration) regimes: (a) phase voltage (blue line) and supply current (green line); (b) DC-capacitor voltage (black line) and DC-line voltage (red line).

As illustrated in Fig. 16 (b), the voltage across the DC-capacitor is kept at its set value of 220 V during the steady-state regimes of active filtering regime and regeneration. The transition to the regeneration regime is accompanied by a low overshoot (about 4 %) generated by the ramp increase of the DC-line voltage, whereas an oscillation of higher amplitude (about 15%) occurs during the transition from the regeneration mode to the active filtering mode due to the rapid decrease of the DC-line voltage. The regeneration regime corresponds to the situation in which $u_C < u_{DC}$, whereas, in active filtering regime, $u_C > u_{DC}$.

B. Experimental Results

The effectiveness of the proposed design method is illustrated through the performance of the system for active filtering and regeneration, named SISFREG, in a laboratory test bench of small scale reproducing the specific conditions of a DC-traction substation with six-pulse diode rectifier.

The electrical scheme is shown in Fig. 17 and the structure of the experimental setup of SISFREG (Fig. 18) illustrates the adopted modular construction, with jump connectors between modules, so that different values of the LCL filter's parameters are available [31].

As shown in Fig. 17, the DC motor (M) is the equivalent of DC-traction motors and the synchronous machine (SM) is the equivalent of the vehicle. SM is connected to the AC power supply and its operation as a generator is equivalent to the traction regime of the DC-traction substation leading to the active filtering-mode of SISFREG. When SM acts as a motor, it is equivalent to the braking regime of the traction motors and the regeneration-mode of SISFREG is expected. The parameters associated to the experimental bench match the values given in the simulation section.

The whole real-time control and monitoring system has been conceived and implemented around a dSPACE 1103 PPC controller board with comprehensive I/O, working together in the Matlab-Simulink environment.

Through the interface between Simulink and DSP, the controller board was fully programmed from the Simulink environment. The acquisition system is based on LEM sensors and provides the analog inputs for the dSPACE platform. The programmable digital I/O channels were used to generate the gating signals for the IGBTs of the three phase VSI and to allow high switching frequencies. A sampling time of 20 μs has been adopted.

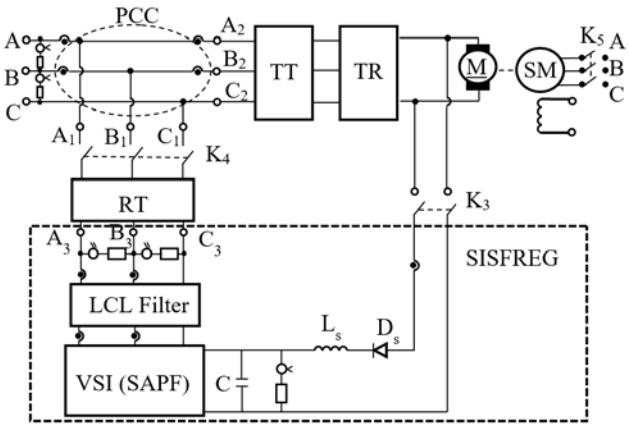

Fig. 17. Scheme of the laboratory setup.

This article has been accepted for publication in a future issue of this journal, but has not been fully edited. Content may change prior to final publication. Citation information: DOI 10.1109/TIA.2018.2819968, IEEE Transactions on Industry Applications

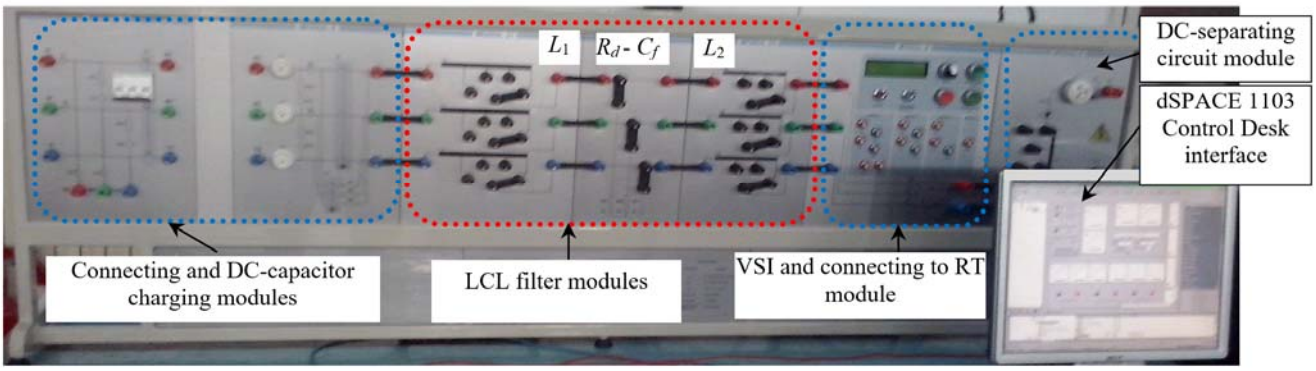

Fig. 18. Structure of the experimental setup of SISFREG.

As illustrated by the waveforms in the conceived Control Desk interface (Fig. 19) and oscillograms (Fig. 20 and Fig. 21), the adopted control strategy and the VSI's AC coupling circuit characterized by C_f=10 μF, R_d=27 Ω, L_1=34 μH, L_2=1.48 mH lead to good harmonic filtering when active power is transmitted to the DC-motor via the six-pulse uncontrolled rectifier.

The associated *THD* of the current drawn from the power supply is about 4.71 % which is below the limit of 5 % specified by IEEE-519 standard [32], even under slightly distorted supply voltage. Taking into consideration the harmonic distortion level of the current in the TT's primary (THD_{iL} = 23.92%), the resulted filtering efficiency is about 5.08. As effect of the reactive power compensation, almost unity power factor (about 0.999) at the fundamental line frequency is illustrated too in Fig. 19 and Fig. 21 through the overlapped waveforms of the phase voltage and current, which are in phase.

The proper operation of the voltage control loop is highlighted through the acquired DC-capacitor voltage shown in the bottom left corner of the Control Desk panel (Fig. 19). It tracks accurately the prescribed value of 220 V leading to the correct generation of the set currents' magnitudes. As shown, their sinusoidal templates of unity magnitude have the same phase as the fundamentals of non-ideal voltages. The waveforms of the currents at the LCL filter input and output are displayed in the top right corner of the Control Desk panel (Fig. 19) and illustrate the effect of the significant attenuation of the switching harmonics.

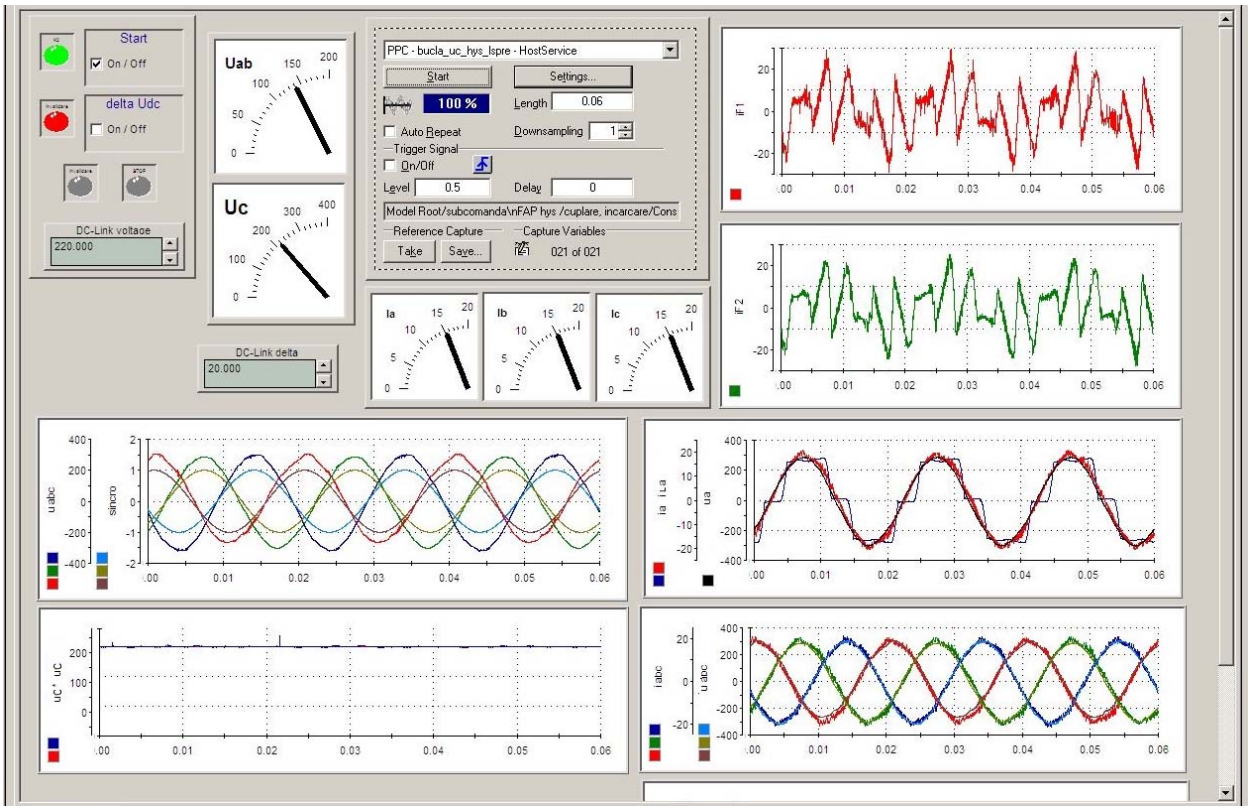

Fig. 19. Control Desk interface for C_f=10 μF, R_d=27 Ω, L_1=34 μH, L_2=1.48 mH in traction regime.

This article has been accepted for publication in a future issue of this journal, but has not been fully edited. Content may change prior to final publication. Citation information: DOI 10.1109/TIA.2018.2819968, IEEE Transactions on Industry Applications

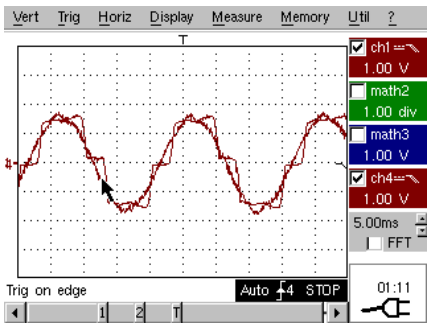

Fig. 20. Oscillograms of currents TT's primary and upstream of PCC for C_f=10 µF, R_d=27 Ω, L_1=34 µH, L_2=1.48 mH in traction regime.

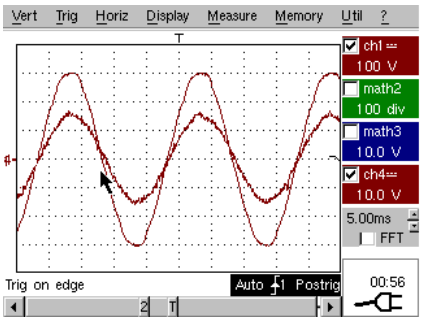

Fig. 21. Oscillograms of phase voltage and current upstream of PCC for C_f=10 µF, R_d=27 Ω, L_1=9 µH, L_2=1.48 mH in traction regime.

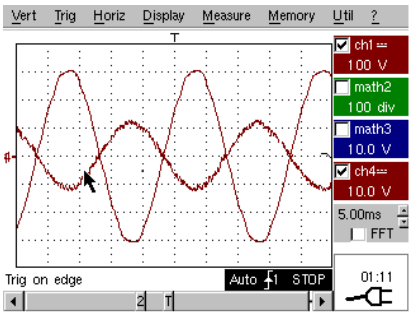

Fig. 22. Oscillograms of phase voltage and current upstream of PCC for C_f=10 µF, R_d=27 Ω, L_1=34 µH, L_2=1.48 mH in regeneration regime.

During the operation in regeneration-mode, the phase opposition between the fundamentals of the supply phase current and voltage is illustrated through the oscillogram of the supply current correlated with the phase voltage (Fig. 22). The current is almost sinusoidal, with a harmonic distortion factor of about 4.85 %.

VIII. Conclusions

A new design method of an LCL filter with damping resistance intended to couple the three-phase VSI of an active DC-traction substation to the power supply has been proposed in this paper. The following elements of originality are outlined.

1) The theoretical substantiation is based on the frequency response from transfer functions related to currents, taking into account the existence of the series damping resistances.
2) The expressed amplitude response and resonance frequency highlight their dependence on only pairs L_2C_f and R_dC_f, It is a very important finding for the conceived design algorithm.
3) The expression of the power losses in the damping resistances is highlighted and an equivalent resistance is introduced as a quantitative indicator of them.
4) By considering the switching frequency as main parameter and taking into consideration the frequency of the highest order harmonic to be compensated, the design algorithm is based on the imposition of the associated attenuations.
5) In the substantiation of the design algorithm, a detailed analysis is performed on the existence of physical-sense solutions, providing the domain in which the values of the parameters must be located.
6) As a large number of parameters values sets can be obtained, a new performance indicator (*MPI*) is proposed, to quantify the extent to which the harmonics to be compensated are influenced.

The analysis and the simulation results achieved for an active DC-traction substation with six-pulse diode rectifier and LCL coupling filter have indicated that the proposed method is valid and effective. The experimental tests conducted in a laboratory test bench of small scale reproducing the specific conditions of a DC-traction substation illustrate good performance of the system for active filtering and regeneration connected to the power supply by the passive damped LCL filter.

The design proposal can be applied in any three-phase LCL-filter-based shunt active power filter.

Acknowledgment

This work was performed through the program Partnerships in priority areas — PN II, conducted with the financial support of MEN – UEFISCDI, project no. PN-II-PT-PCCA-2013-4-0564 (42/01.07.2014).

References

[1] A. Ghoshal and V. John, "Active damping of LCL filter at low switching to resonance frequency ratio," *IET Power Electron.*, vol. 8, no. 4, pp. 574–582, 2015.

[2] G. E. Mejia Ruiz, N. Munoz, and J. B. Cano, "Modeling, analysis and design procedure of LCL filter for grid connected converters," in *Proc. 2015 IEEE Workshop Power Electron. and Power Quality Appl. (PEPQA)*, pp. 1–6.

[3] M. Hanif, V. Khadkikar, W. Xiao, and J. L. Kirtley, "Two degrees of freedom active damping technique for filter-based grid connected PV systems," *IEEE Trans. Ind. Electron.*, vol. 61, no. 6, pp. 2795–2803, June 2014.

[4] X. Wang, F. Blaabjerg, and P. C. Loh, "Grid-current-feedback active damping for LCL resonance in grid-connected voltage source converters," *IEEE Trans. Power Electron.*, vol. 31, pp. 213–223, 2016.

[5] W. Xia, J. Kang, "Stability of LCL-filtered grid-connected inverters with capacitor current feedback active damping considering controller time delays," *J. Mod. Power Syst. Clean Energy*, vol. 5, no. 4, pp. 584–598, July 2017.

[6] M. B. Said-Romdhane, M. W Naouar, I.. S. Belkhodja, and E Monmasson, "An improved LCL filter design in order to ensure stability without damping and despite large grid impedance variations," *Energies*, vol. 10, no. 3, pp. 336, Mar. 2017.

[7] A. Reznik, M.G. Simões, A. Al-Durra, and S.M. Muyeen, "LCL filter design and performance analysis for grid-interconnected systems," *IEEE Trans. Ind. Appl.*, vol. 50, no. 2, pp. 1225–1232, Mar./Apr. 2014.

[8] S. Jayalath .and M. Hanif, "Generalized LCL-filter design algorithm for grid-connected voltage-source inverter", *IEEE Trans. Ind. Electron*., vol. 64, no. 3, pp. 1905–1915, Mar. 2017.

[9] R. N. Beres, X. Wang, M. Liserre, F. Blaabjerg, and C. L. Bak, "A review of passive power filters for three-phase grid-connected voltage-source converters," *IEEE J. Emerg. Sel. Topics Power Electron*, vol. 4, no. 1, pp. 54–69, Mar. 2016.

[10] J. Fang, H. Li, and Y. Tang, "A magnetic integrated LLCL filter for grid-connected voltage-source converters, *IEEE Trans. Power Electron*., vol. 32, no. 3, pp. 1725–1730, Mar. 2017.

[11] M. Liserre, F. Blaabjerg, and S. Hansen, "Design and control of an LCL-filter-based three-phase active rectifier," *IEEE Trans. Ind. Appl*., vol. 41, no. 5, pp. 1281–1291, Sept./Oct. 2005.

[12] K.-B. Park, F.D. Kieferndorf, U. Drofenik, S. Pettersson, and F. Canales, "Weight minimization of LCL filters for high-power converters: impact of PWM method on power loss and power density," *IEEE Trans. Ind. Appl*., vol. 53, no. 3, pp. 2282–2296, May/June 2017.

[13] B. Hoff and W. Sulkowski, "Grid-connected VSI with LCL filter—models and comparison," *IEEE Trans. Ind. Appl*., vol. 50, no. 3, pp. 1974–1981, May/June 2014.

[14] M. T. Bina and E. Pashajavid, "An efficient procedure to design passive LCL-filters for active power filters," *Elect. Power Syst. Res.*, vol. 79, no. 4, pp. 606–614, Apr. 2009.

[15] L. Li, Y. Guo, and X. Zhang, "Analysis and application of passive damping LLCL filter in active power filter," in *Proc. 2015 IEEE Conf. CYBER*, pp. 751–755.

[16] Y. Tang, P. C. Loh, P. Wang, F. H. Choo, F. Gao, and F. Blaabjerg, "Generalized design of high performance shunt active power filter with output LCL filter," *IEEE Trans. Ind. Electron*., vol. 59, no. 3, pp. 1443–1452, Mar. 2012.

[17] N. Yu, J. Yang, S. Chen, and M. Ye, "Design of LCL-filter based three-level active power filters," *TELKOMNIKA Indonesian J. Electr. Eng.*, vol. 12, no. 1, pp. 48–56, Jan. 2014.

[18] Q. Liu, L. Peng, Y. Kang, S. Tang, D. Wu, and Y. Qi, "A novel design and optimization method of an LCL filter for a shunt active power filter," *IEEE Trans. Ind. Electron*., vol. 61, no. 8, pp. 4000–4010, 2014.

[19] A. Terciyanli, A. Acik, A. Cetin, M. Ermis, et al, "Power quality solutions for light rail public transportation systems fed by medium-voltage underground cables", *IEEE Trans. Ind. Appl*., vol. 48, no. 3, pp. 1017–1029, May/June 2012.

[20] W.A.G. de Jager, M. Huizer, and E.K.H. van der Pols, "Implementation of an active regeneration unit in a traction substation," in *Proc. EPE'14-ECCE Europe*, pp. 1–9, Aug. 2014.

[21] S. Lim and J. Choi, "LCL filter design for grid connected NPC type three-level inverter," *Int. J. Renew. Energy Res.*, vol. 5, no. 1, 2015.

[22] A. Reznik, M. G. Simoes, A. Al-durra, S. M. Muyeen, "LCL Filter design and performance analysis for small wind turbine systems," in *Proc. 2012 Power Electron. and Mach. in Wind Appl.*, pp. 1–7.

[23] M. Huang, F. Blaabjerg, Y. Yang, W. Wu, "Step by step design of a high order power filter for three-phase three-wire grid-connected inverter in renewable energy system," in *Proc. 4th IEEE PEDG*, 2013.

[24] C. Liu, K. Dai, K. Duan, Y. Kang, "Application of a C-type filter based LCFL output filter to shunt active power filters," *J. Power Electron*, vol. 13, no. 6, pp. 1058–1069, Nov. 2013.

[25] M. Popescu, A. Bitoleanu, V. Suru, and A. Preda, "System for converting the DC traction substations into active substations," in *Proc. 2015 9th Int. Symp. on Advanced Topics in Elect. Eng. (ATEE),* pp. 632–637.

[26] M. Popescu, A. Bitoleanu, and V. Suru, "Indirect current control in active DC railway traction substations," in *Proc. ACEMP-OPTIM-ELECTROMOTION Joint Conference*, pp. 192–197, Sept. 2015.

[27] M. Popescu, A. Bitoleanu, and V. Suru, "On the design of LCL filter with passive damping in three-phase shunt active power filters," in *Proc. 2016 IEEE Int. Symp. Power Electron,, Electr. Drives, Automation and Motion (SPEEDAM)*, pp. 826-831.

[28] M. Popescu, A. Bitoleanu, and A. Preda, "A new design method of an LCL filter in active DC-traction substations," in *Proc. 2016 IEEE Int. Power Electron. and Motion Control Conf. and Expo. (PEMC)*, Varna, Bulgaria, 25-30 Sept. 2016, pp. 876–881.

[29] A. Bitoleanu, M. Popescu, C.V. Suru, "Theoretical and experimental evaluation of the indirect current control in active filtering and regeneration systems," in *Proc. OPTIM-ACEMP Joint Conference* 2017, pp. 759-764, May 2017.

[30] A. Bitoleanu, M. Popescu, D. Marin, and M. Dobriceanu, "LCL interface filter design for shunt active power filters," *Advances in Electrical and Computer Engineering*, vol. 10, pp. 55–60, Aug. 2010.

[31] M. Popescu, A. Bitoleanu, and M. Dobriceanu, "Investigations on the coupling LCL filter in active traction substations", in *Proc. 2017 IEEE Int. Conf. OPTIM & ACEMP*, pp. 654–659.

[32] *IEEE Recommended Practice and Requirements for Harmonic Control in Electrical Power Systems*, IEEE Std. 519-1992.